

# KeyVID: Keyframe-Aware Video Diffusion for Audio-Synchronized Visual Animation

Xingrui Wang<sup>1,2</sup> Jiang Liu<sup>1</sup> Ze Wang<sup>1</sup> Xiaodong Yu<sup>1</sup> Jialian Wu<sup>1</sup>  
 Ximeng Sun<sup>1</sup> Yusheng Su<sup>1</sup> Alan Yuille<sup>2</sup> Zicheng Liu<sup>1</sup> Emad Barsoum<sup>1</sup>  
<sup>1</sup>Advanced Micro Devices <sup>2</sup>Johns Hopkins University

## Abstract

Generating video from various conditions, such as text, image, and audio, enables both spatial and temporal control, leading to high-quality generation results. Videos with dramatic motions often require a higher frame rate to ensure smooth motion. Currently, most audio-to-visual animation models use uniformly sampled frames from video clips. However, these uniformly sampled frames fail to capture significant key moments in dramatic motions at low frame rates and require significantly more memory when increasing the number of frames directly. In this paper, we propose KeyVID, a keyframe-aware audio-to-visual animation framework that significantly improves the generation quality for key moments in audio signals while maintaining computation efficiency. Given an image and an audio input, we first localize keyframe time steps from the audio. Then, we use a keyframe generator to generate the corresponding visual keyframes. Finally, we generate all intermediate frames using the motion interpolator. Through extensive experiments, we demonstrate that KeyVID significantly improves audio-video synchronization and video quality across multiple datasets, particularly for highly dynamic motions. The code is released in <https://github.com/XingruiWang/KeyVID>.

## 1. Introduction

Recent years have witnessed remarkable progress in video generation, driven by advancements in diffusion-based models [3, 4, 6, 7, 12, 16, 17, 21, 22, 41, 55, 59]. These frameworks typically condition the generation process on *text* prompts and/or *image* inputs, where the text provides semantic guidance (e.g., actions, objects, or stylistic cues), while the image specifies spatial composition (e.g., object layout, scene structure or visual styles). Despite their success, these methods largely focus on aligning visual outputs with static text or image, leaving dynamic, time-sensitive modalities such as *audio* underexplored.

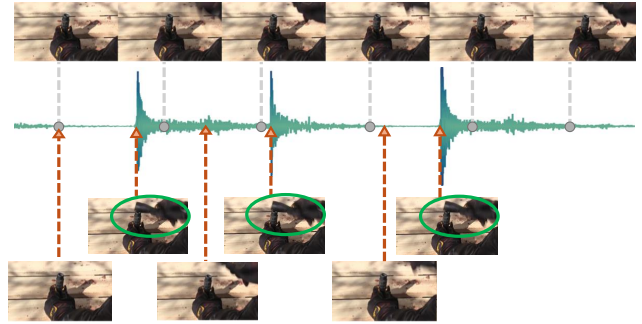


Figure 1. *Top*: Uniformly sampled sparse frames, which fail to capture the key moments evident in the corresponding audio (*Middle*). *Bottom*: Key frames precisely aligned with the hammer striking down, matching the critical moments in the audio waveform.

Audio-Synchronized Visual Animation (ASVA) [66] is a task that aims to animate objects in a natural static image into a video with motion dynamics that are semantically aligned and temporally synchronized with the input audio. It utilizes audio cue to provide more fine-grained semantic and temporal control for video generation, which requires a deep understanding of audio semantics, audio-visual correlations and object dynamics. To achieve precise audio-visual synchronization in ASVA, it is crucial to align key visual actions accurately with their corresponding audio signals. For example, given an audio clip of hammering sounds, the hammer in the video should strike the nail at the exact moment the impact sound occurs. However, this synchronization is constrained by the frame rates of video generation models. For example, AVSyncD [66] trains and generates videos at 6 FPS, posing a significant challenge for audio-synchronized video generation. Since audio carries fine-grained temporal information, the key moments in the audio can be lost in uniformly sampled low frame rate videos (see Fig. 1), leading to compromising audio-video synchronization.

A straightforward solution is to train a video generation model on high frame rate data to match the fine-grained

temporal information in audio. However, this approach incurs substantial computational costs in terms of GPU memory and training time. To alleviate this, in video generation it is common to adopt a two-stage strategy that first generates low frame rate videos and then applies frame interpolation to obtain high frame rate videos [3, 20, 41], or a random frame rate strategy that uses random frame sampling rates while maintaining a small, fixed number of frames during training [41, 68]. However, the two-stage approach struggles in modeling highly dynamic sequences, where critical events may be lost due to the sparsity of the initial uniform frames, and the random frame rate strategy fails to model long-term temporal dependency at high frame rates.

To ensure accurate audio-visual synchronization while maintaining computation efficiency, we propose **KeyVID**, a **Keyframe-aware Video Diffusion** framework that generates audio-synchronized video based on the input image and audio. We first develop a keyframe selection strategy that identifies critical moments in the video sequence based on an optical flow-based motion score. We train a *keyframe localizer* that predicts such keyframe positions directly from the input audio cue. Next, instead of applying uniform downsampling to video frames, we select the keyframes to train a *keyframe generator*. The keyframe generator explicitly captures crucial moments of dynamic motion that might otherwise be missed with uniform sampling without requiring an excessively high number of frames. Then, we train a specialized *motion interpolator* to synthesize intermediate frames between the keyframes to generate high frame rate videos. The motion interpolator ensures smooth motion transition and precise audio-visual synchronization throughout the sequence. This approach is similar to how the animation industry creates smooth and dynamic movements, where the *Key Animator* establishes key moments in a scene and the *Inbetweener* fills in the gaps to ensure that the movements appear seamless and fluid. The overall generation pipeline of KeyVID is shown in Fig. 2.

We conducted extensive experiments across diverse datasets featuring varying degrees of motion dynamics and audio-visual synchronization. We demonstrate that our keyframe-aware approach outperforms state-of-the-art methods in video generation quality and audio-video synchronization. In particular, on the AVSync15 dataset [66], we achieve an FVD score [49] of 262.3, and a RelSync score [66] of 48.33, outperforming the state-of-the-art by absolute margins of **86.8**, and **2.81**, respectively. Our user study demonstrates a clear preference towards videos generated by KeyVID over those produced by baseline methods.

The main contributions of our work are as follows:

- We propose a keyframe-aware audio-to-visual animation framework that first localizes keyframe positions from the input audio and then generates the corresponding video keyframes using a diffusion model.

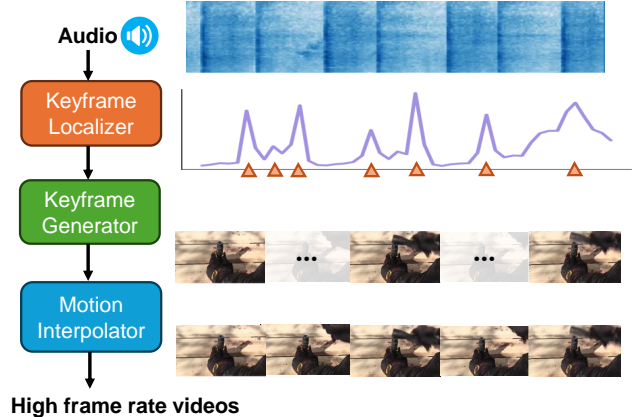


Figure 2. KeyVID video generation pipeline.

- We introduce a motion interpolation network that synthesizes intermediate frames between keyframes, enabling high frame rate video generation with smooth motion while maintaining memory efficiency.
- Comprehensive experiments demonstrate our superior performance in audio-synchronized video generation, particularly in highly dynamic scenes with distinct audio-visual events.

## 2. Related Work

### 2.1. Video Diffusion Models

Diffusion models [3, 4, 6, 7, 12, 16, 17, 21, 22, 41, 55, 59] emerge as powerful tools to generate high-quality videos. For the data sample  $\mathbf{x}_0 \sim p_{\text{data}}(\mathbf{x})$ , Gaussian noise is added over  $T$  steps, creating a noisy version  $\mathbf{x}_T$ . A model  $\epsilon_\theta$  is trained to invert this process by predicting and subtracting the noise by minimizing:

$$\min_{\theta} \mathbb{E}_{t, \mathbf{x} \sim p_{\text{data}}, \epsilon \sim \mathcal{N}(0, I)} [\|\epsilon - \epsilon_\theta(\mathbf{x}_t, t)\|_2^2]. \quad (1)$$

For latent video generation [4, 17, 55, 63],  $\mathbf{x} \in \mathbb{R}^{L \times 3 \times H \times W}$  is encoded into a latent vector  $\mathbf{z} \in \mathbb{R}^{L \times C \times h \times w}$  using an encoder  $\mathcal{E}(\cdot)$  to reduce computation, where  $C$  is the latent dimension and  $L$  is the number of frames. The noise-adding diffusion process and the learned reverse process are conducted on  $\mathbf{z}$  instead. Recent advancements in video diffusion models leverage pre-trained text encoders [36, 37] to inject text conditions into the denoising process for text-to-video generations [4, 6, 22, 32]. Moreover, image conditioning can also be introduced to enhance video generation by providing visual features that control the visual contents [8, 30, 51, 53, 57] or frame conditions [2, 7, 13, 16, 50, 55, 65]. By adding condition  $\mathbf{c}$  to the denoising process, the objective becomes:

$$\min_{\theta} \mathbb{E}_{\mathbf{z}, \epsilon \sim \mathcal{N}(0, 1), t} [\|\epsilon - \epsilon_\theta(\mathbf{z}_t, t, \mathbf{c})\|_2^2]. \quad (2)$$

### 2.2. Audio-to-Video Generation

Compared to text and image, audio can not only provide semantic guidance to video generation, but also provide fine-grained temporal guidance for motion generation. Early works have explored

audio-conditioned video synthesis for domain-specific tasks on human body on both 2D motion generation [9, 42, 43, 54, 58, 64], and 3D motion synthesis [31, 33, 38, 44]. Benefiting from pre-trained audio feature extractors [10, 11, 15], current studies have incorporated audio signals into general video generation. For general video synthesis, some approaches [18, 23, 25, 45–47, 52] have utilized audio as a global feature for overall style or semantic control, and other works [24, 27, 29, 39, 60] consider temporal alignment between the generated video and the input audio. Recently, Zhang et al. [66] introduced the higher quality audio video synchronized dataset and incorporated time dependent audio features to enable finer temporal control over motion generation using audio clips. However, the quality of generated motion are still limited by the low frame rate setting, especially for high dynamical motions. At the same time, increase the densities of frames the uniform sample are requires expensive resource for training.

### 2.3. Keyframe-based Video Processing

In video processing, keyframes are pivotal in compressing video clips or motions by retaining essential features, thereby facilitating efficient analysis of lengthy videos or high-dynamic motions [1, 26, 28, 40, 56]. In the realm of video generation, keyframes serve as foundational references, enabling the synthesis of intermediate frames that ensure temporal coherence and visual consistency. For long video generation, current approaches employ keyframe-based generation pipelines to enhance long-term coherence in video synthesis [62, 67]. Others focus on interpolation techniques from keyframes, which predict missing frames between keyframes input, ensuring motion realism and visual consistency in dynamical motions [14].

## 3. Methods

In this section, we present our keyframe-aware, audio-conditioned video generation framework **KeyVID**. Given an input audio and the first frame of a video, we follow a three-stage generation process (Fig. 2) and train three separate models: (1) **Keyframe Localizer** – Predicting a motion curve from the input audio and detecting the keyframe positions (Sec. 3.1); (2) **Keyframe Generator** – Generating keyframe images at detected keyframe positions conditioned on the input image and audio (Sec. 3.2); (3) **Motion Interpolator** – Synthesizing intermediate frames to reconstruct a smooth video with dense frames conditioned on the generated keyframe images and input audio. (Sec. 3.3). Our

### 3.1. Keyframe Localization from Audio

We first train a *keyframe localizer* to infer keyframe locations from audio features by exploiting the correlation between acoustic events and motion changes. For instance, a hammer striking a table generates a sharp sound that often aligns with a sudden visual transition.

**Optical Flow based Motion Score.** To train this localizer, we first generate keyframe labels by analyzing optical flow from training video sequences, as shown in Fig. 3. These labels provide supervision for training a keyframe detection network that predicts keyframe positions from audio input. The network learns the underlying relationship between motion dynamics and acoustic cues,

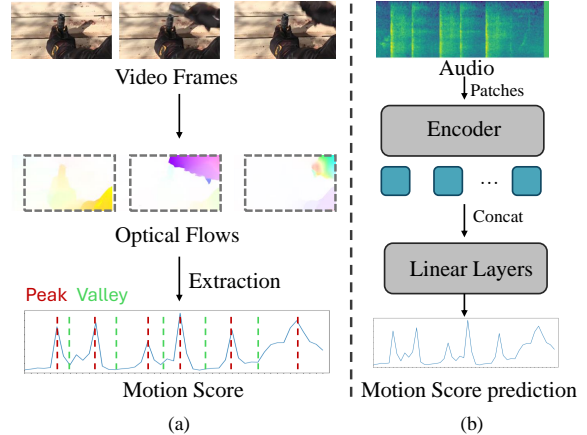


Figure 3. (a) We first calculate the optical flow and then take the average across all pixels for each frame to form a curve of motion score. The peaks (red) and valleys (green) indicate key frames. (b) key frame prediction network from audio, described in Sec. 3.1.

imposing keyframe awareness in video generation relying only on audio signals.

As shown in Fig. 3(a), we first obtain the “motion score” for each frame by calculating the optical flow and then averaging it across all pixels. These scores collectively form a temporal motion curve across the frame sequence. Specifically, we employ a pre-trained RAFT model [48] as the optical flow estimator. Given a video clip consisting of frames  $\{I_t\}_{t=1}^T$ , RAFT computes the optical flow field  $\mathbf{OF}_t$  between two frames  $I_t$  and  $I_{t+1}$ . The optical field consists of horizontal ( $u_t$ ) and vertical ( $v_t$ ) components at each pixel, where  $t = 1, \dots, T - 1$ . The motion score  $M(t)$  of the frame  $t$  is then computed as:

$$M(t) = \sum_{i,j} (|u_t(i,j)| + |v_t(i,j)|), \quad (3)$$

where  $t$  denotes the timestep of the video sequence, and  $(i,j)$  represents the location of each pixel.

**The structure of keyframe localizer** As shown in Fig. 3(b), the keyframe localizer processes raw audio by converting it into a spectrogram and extracting features using a pretrained transformer-based encoder to predict motion score supervised by ground truth  $M(t)$  calculated by optical flow. To better align the extracted features with the temporal resolution of motion cues, we modify the preprocessing stride and interpolate positional embeddings, as detailed in the Appendix A. The processed audio features are then passed through fully connected layers to predict a sequence of confidence scores representing keyframe likelihoods over time. The model is trained using an L1 loss with the ground-truth motion score derived from optical flow analysis.

### 3.2. Audio-conditioned Key Frame Generation

We train a *keyframe generator* to generate  $T_K$  keyframes for a video sequence of length  $T$ , conditioned on audio, the first frame, and text descriptions as shown in Fig. 4. Unlike previous video generation models [55, 66] that are trained on uniformly down-sampled frames, our method exploits a keyframe selection process to identify motion-related frames during training for reducing

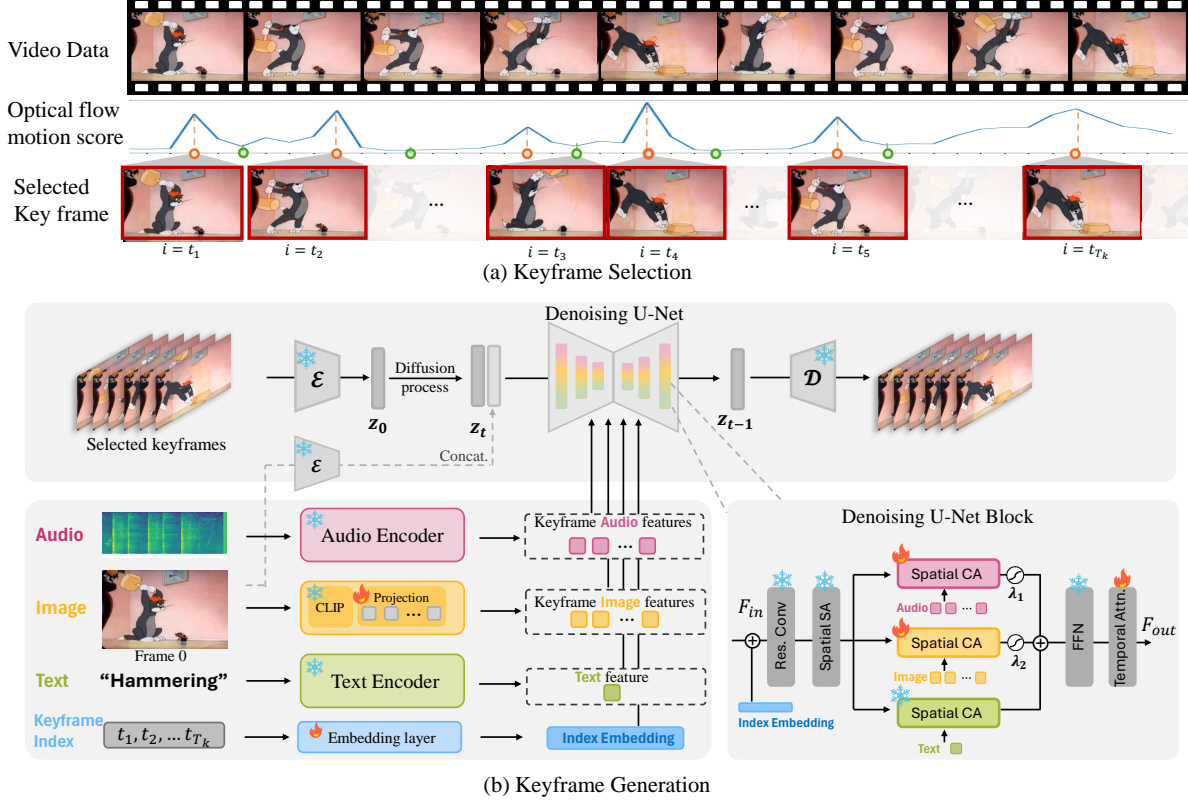


Figure 4. (a) The key frame data selection and (b) the diffusion model for audio conditioned keyframe generation pipeline. (a) From the original video clips, we first calculate the curve of the motion score from the optical flow of each frame in Sec. 3 and select the key frames from the curve (b) We train a video diffusion model to generate these sparse frames conditioned on the audios, first frame image, text, with additional keyframe index. These condition are processed by their encoder and passed into the denoising U-Net. The index embedding are added with video features and passed into Residual convolutional block (**Res. Conv.**). The following layers contain a spatial self-attention (**SA**) and spatial cross attention (**CA**) on each three conditional features. The output of each CA are followed by a gating with learnable weights  $\lambda$ . Please see details in Sec. 3.2.2.

training cost and capturing crucial motions. We build a diffusion model to generate keyframes with their corresponding audio, image, text features, as well as frame indices to provide accurate conditions during generation.

### 3.2.1. Keyframe Data Selection

We compute the motion score  $M(t)$  for frames and select  $T_K \ll T$  keyframes to train the diffusion model based on the peaks and valleys of the motion score sequence. We need to make sure the selected keyframes cover most of peaks and valleys. We first select the first frame and randomly choose  $\frac{T_K}{2} - 1$  peaks from all detected peaks. If the total number of detected peaks is less than  $\frac{T_K}{2} - 1$ , we include all of them. Second, we select one valley between each pair of consecutive selected peaks to ensure the completeness of motion. The remaining keyframes are selected by evenly sampling from frame indices based on the size of adjacent bins. This strategy ensures that for sequences with smooth motion or weak audio signals, where the number of peaks and valleys is limited, the selection process approximates uniform down-sampling, making the training setup more consistent with standard video diffusion models. The details of this process and keyframes

example are included in the Appendix A and D.

The selected  $T_K$  key frames will be the data to train the diffusion model. The keyframe indices,  $\{t_1, t_2, \dots, t_{T_K}\}$ , serve as additional conditions to the generation process.

### 3.2.2. Keyframe Generator Architecture

The keyframe generator introduces two key enhancements: (1) **Frame index embedding** - A keyframe index embedding encodes each frame’s absolute position, ensuring coherence when generating non-uniformly distributed frames. (2) **Feature conditions** - The model is conditioned on **audio, image and text** features. The audio and image features are extracted from corresponding keyframe time windows (e.g., a hammer strike or a gunshot).

As shown in Fig. 4(b), the diffusion process and denoising network are built on the latent features of selected keyframes following common latent diffusion model design [3, 4], and the encoder and decoder are pretrained from Xing et al. [55] and frozen. In the denoising process of the diffusion model, the latent features of video frames are represented as  $\mathbf{z} \in \mathbb{R}^{B \times T_k \times C \times h \times w}$ , where  $B$  denotes the batch size,  $T_k$  the number of frames at each denoising step,  $h$  and  $w$  the spatial dimensions, and  $C$  the feature channels.

**Frame Index Embedding.** Off-the-shelf video diffusion models, assuming uniformly sampled frames, cannot directly handle sparsely distributed keyframes. To address this, we introduce a frame index embedding layer that encodes the absolute index of each keyframe within the original video sequence. The keyframe indices are represented as a vector  $\{i_t\}_{t=1}^{T_K}$  of length  $T_K$ , where each  $i_t$  corresponds to the a selected keyframe. During the denoising process, the latent features of video frames are represented as  $\mathbf{z} \in \mathbb{R}^{B \times T_K \times C \times H \times W}$ . The frame index embedding  $\mathbf{f}_{\text{emb}} \in \mathbb{R}^{B \times T_K \times C}$  is added up with the latent features  $\mathbf{z}$  before passing them into the denoising U-Net, ensuring explicit positional information is provided to the network when generating non-uniformly distributed frames.

**Audio Feature Conditions.** We use a pretrained ImageBind encoder [15] to extract audio features for video synthesis. Given an input spectrogram  $\mathbf{A} \in \mathbb{R}^{C_A \times T_A}$ , the encoder splits it into overlapping patches of size  $(c_a, t_a)$  with a stride  $\Delta t < t_a$  and encodes it into a sequence of embeddings  $\{\mathbf{h}_i\}_{i=1}^{N'}$  using a transformer-based architecture. The audio encoder output two type of tokens: one global token  $\mathbf{h}_{\text{global}}$  captures high-level semantic information, and local tokens retain fine-grained temporal details.

Since the diffusion model operates on  $T_K$  sparsely selected keyframes, we first segment the extracted audio features into  $T$  time steps to match the full video length, resulting in  $\mathbf{f}_{\text{audio}} \in \mathbb{R}^{B \times T \times C \times N}$ . Using the keyframe indices  $\{i_t\}_{t=1}^{T_K}$ , we extract the corresponding  $T_K$  audio features from the full  $T$ -length sequence. These embeddings are fused with text and image conditions via cross-attention layers in the U-Net, ensuring accurate synchronization between generated frames and their associated audio cues.

**Image Feature Conditions.** We extract image features using a pretrained vision encoder, following prior work [55]. The first frame of the video is processed through a frozen CLIP [36] model to obtain the feature representation  $\mathbf{f}_{\text{img}}$ . A projection layer with  $t$  tokens transform this feature to match the temporal length of  $\mathbf{z}$ . To align with keyframe-based generation, we expand the temporal dimension to  $T$  and extract image embeddings for all  $T$  frames, yielding  $\mathbf{f}_{\text{img}} \in \mathbb{R}^{B \times T \times C \times H \times W}$ . We then select the corresponding  $T_K$  features using keyframe indices  $\{i_t\}_{t=1}^{T_K}$ .

**Text Feature Conditions.** Following prior work, we encode the textual description using a frozen CLIP model ([36]. The extracted text embedding is repeated for all  $T_K$  keyframe to provide consistent semantic guidance during the denoising process.

**Feature Fusion.** Each conditioning feature (audio, image, and text) is processed separately through spatial cross-attention layers. The input query is shared across all modalities. Following DynamiCrafter [55], we integrate audio features with other conditioning modalities. Given input latent features  $\mathbf{F}_{\text{in}}$ , we compute query projections  $\mathbf{Q} = \mathbf{F}_{\text{in}} \mathbf{W}_Q$  and apply spatial attention to text, image, and audio features:

$$\begin{aligned} \mathbf{F}_{\text{out}} = & \text{SpatialAttention}(\mathbf{Q}, \mathbf{K}_{\text{txt}}, \mathbf{V}_{\text{txt}}) \\ & + \lambda_1 \cdot \text{SpatialAttention}(\mathbf{Q}, \mathbf{K}_{\text{aud}}, \mathbf{V}_{\text{aud}}) \\ & + \lambda_2 \cdot \text{SpatialAttention}(\mathbf{Q}, \mathbf{K}_{\text{img}}, \mathbf{V}_{\text{img}}). \end{aligned} \quad (4)$$

where  $\mathbf{K}$  and  $\mathbf{V}$  are the key and value projections for each modality, and  $\lambda_1, \lambda_2$  are learnable fusion weights [55]. The fused features are then processed through a feedforward network (FFN) and temporal self-attention to ensure spatial and temporal consistency.

### 3.3. Motion Interpolator

After generating  $T_K$  keyframes, we use a *motion interpolator* to generate the missing frames back to the full video sequence of length  $T$ . Interpolation has been widely used in uniform frame generation [3, 55], where a model predicts a fixed number of intermediate frames given the first and last frame. However, for keyframe-based generation, the positions of missing and available frames vary, introducing additional challenges.

To address this, we adapt our *keyframe generator* diffusion model into a *motion interpolator* model that generates  $T_K$  frames at once using masked frame conditioning. The overall architecture remains nearly unchanged, with the primary difference lying in how image conditions are incorporated. Rather than conditioning solely on the first frame, the model utilizes the features of generated keyframes as conditions, thereby learning to synthesize the missing frames in between. This approach facilitates interpolation between non-uniformly distributed keyframes while maintaining temporal consistency. A pipeline can be found in Appendix C.

To generate a full video with  $T$  frames in a single pass, we incorporate FreeNoise [35] to increase the number of output frames during inference. This allows the interpolation model to take all generated keyframes as conditioning inputs and predict all missing frames in one single step. Further details on the training and inference time of this model are provided in the Appendix G.

## 4. Experiments

### 4.1. Implementation Details

**Datasets.** We evaluate our method on three datasets, *AVSync15* [66], *Landscapes* [29], and *TheGreatestHits* [34]. *AVSync15* is a subset of the VGG-Sound [5] dataset, consisting of fifteen classes of activities with highly synchronized audio and video captured in the wild. Some activities have more intense motions, such as hammer hitting and capgun shooting. *Landscapes* is a collection of natural environment videos with corresponding ambient sounds without synchronized video motion. *TheGreatestHits* contains videos of humans hitting various objects with a drumstick, producing hitting sounds that are temporally aligned with the motions. We sample 2 second audio-video pairs from these datasets for experiments. Videos were sampled at 24 fps with 48 frames, and resized to  $320 \times 512$ . Audios were sampled at 16kHz and converted into 128-d spectrograms. We set  $T_K = 12$  temporal length of key frame generation and interpolations.

**Training.** We adopted the pre-trained DynamiCrafter [55] as the backbone video diffusion model and pre-trained ImageBind [15] as the audio encoder. All models were trained using Adam optimizer with a batch size of 64 and a learning rate of  $1 \times 10^{-5}$ .

**Baselines.** We follow [66] to compare our method with the simple *static* baseline where the input frame is repeated to form a video, as well as state-of-the-art video generation models with different input modalities: (1) **T+A** is the video generation model based only on text and audio, such as TPoS [23] and TempoToken [61]. (2) **I+T** includes many state of the art video generation models, which conditioned on images and text prompt. We compare VideoCrafter [6], I2VD [66] and DynamiCrafter [55]. We also compare the DynamiCrafter tuned on the target dataset without audio input for the fair comparison. (3) **I+T+A**. The models take

Input	Model	AVSync15						Landscapes					
		FID↓	IA↑	IT↑	FVD↓	AlignSync↑	RelSync↑	FID↓	IA↑	IT↑	FVD↓	AlignSync↑	RelSync↑
T+A	TPoS [23]	13.5	23.38	24.83	2671.0	19.52	42.50	16.5	15.61	26.70	2081.3	23.12	48.15
	TempoToken [61]	12.2	18.84	17.45	4466.4	19.74	44.05	16.4	22.58	22.87	2480.0	24.21	48.65
I+T	I2VD [66]	12.1	-	30.35	398.2	21.80	43.92	16.7	-	22.56	539.5	24.74	49.89
	DynamiCrafter [55]	11.7	-	30.02	400.7	21.76	43.68	23.51	-	21.95	445.8	24.17	49.63
I+T+A	CoDi [46]	14.5	28.15	23.42	1522.6	19.54	41.51	20.5	22.63	<b>24.23</b>	982.9	22.63	45.48
	TPoS [23]	11.9	38.36	<b>30.73</b>	1227.8	19.67	39.62	16.2	<b>23.52</b>	23.20	789.6	23.51	47.05
	AADiff [27]	18.8	34.23	28.97	978.0	22.11	45.48	70.7	22.07	22.92	1186.3	<b>26.77</b>	<b>53.93</b>
	AVSyncD [66]	11.7	38.53	30.45	349.1	22.62	45.52	<b>16.2</b>	22.49	22.79	415.2	24.82	49.93
	<b>KeyVID (Ours)</b>	<b>11.00</b>	<b>39.23</b>	30.30	<b>262.3</b>	<b>24.08</b>	<b>48.33</b>	23.28	19.85	21.44	<b>391.0</b>	24.35	49.95
Static	-	39.76	30.39	1220.4	21.83	43.66	-	23.60	22.21	1177.5	25.79	51.59	
Groundtruth	-	40.06	30.31	-	25.04	50.00	-	23.65	22.08	-	25.01	50.00	

Table 1. Performance on AVSync15 and Landscapes.

image, text and audio for video generation as our model, which includes CoDi [47], TPoS [24], AADiff [27] and AVSyncD [66].

**Metrics.** We use the Frechet Image Distance (FID) [19] and Frechet Video Distance (FVD) [49] to evaluate the visual quality and temporal coherence of synthesized videos. For the semantic alignment between each text and audio domain to the generation result, we compare the average image-text (IT) and image-audio (IA) scores of frames in a video with CLIP [36] and ImageBind [15]. As one of our research concentration, we evaluate the audio synchronization score with the generated video with RelSync and AlignSync proposed by Zhang et al. [66].

## 4.2. Quantitative results

Table 1 presents the results on the AVSync15 and the Landscapes datasets. On AVSync15, our KeyVID outperforms other methods in terms of audio-visual synchronization, achieving the highest AlignSync (24.09) and RelSync (48.30) scores. This demonstrates the effectiveness of our keyframe selection strategy in capturing crucial dynamic moments that align with audio events. Our method also achieves competitive performance in visual quality metrics (FID is 11.0 and FVD is 262.3), outperforming the previous best method AVSyncD. The Landscapes dataset has much less dynamics without synchronized and only used for evaluating visual quality. Compared with others baseline, our method achieves the lowest FVD score (391.09). The synchronization metrics are similar to others – the AlignSync is 24.35 and RelSync is 49.95. Those demonstrate our method achieve better visual quality compared with baseline models.

In Table 2, we present results on TheGreatestHits dataset, which features distinct percussive audio events temporally aligned with visual motions. Our approach achieves the best performance across all metrics, with notable improvements in audio-visual synchronization compared to AVSyncD, where the AlignSync score improved by 24.09 and RelSync achieve 49.12.

## 4.3. Visualization

Figure 5 presents qualitative comparisons between our method and baseline approaches. Our keyframe-aware approach more accurately captures motion peaks that align with audio events, such as the exact moment of impact in hammering or the smoke in gun shooting. Compared to uniform frame sampling, our method bet-

ter preserves temporal coherence by focusing on key moments of motion. In sequences like dog barking and lion roaring, KeyVID-Keyframe ensures that mouth movements align precisely with sound peaks, whereas uniform sampling and AVSyncD introduce temporal misalignment or missing frames. Similarly, in frog croaking and baby crying, facial and mouth movements are better synchronized with the audio, demonstrating the effectiveness of keyframe-aware training across both high- and low-intensity motion scenarios. Additional visualizations are provided in the supplementary.

## 4.4. Ablation Study

To validate our introduction of keyframe awareness in the audio to video generation task, we conducted ablation studies. Table 3 compares the performance of generating keyframe first then interpolate versus the one with traditional uniform frames. We evaluate them on two setting: (1) Downsample our output to 12 uniform frames and compare with the 12 uniform frames directly generate by baseline. (2) Compare our results with the 48 frames interpolated from the 12 uniform frames of baseline to with the same method in Sec. 3.3.

We observe that keyframe selection significantly outperforms uniform sampling in both settings, with larger improvements in the synchronization metrics (AlignSync and RelSync). This confirms our hypothesis that strategically selecting keyframes based on audio and motion cues leads to better temporal alignment between audio events and visual dynamics.

## 4.5. Efficiency Analysis

To evaluate KeyVID’s efficiency, we compare its memory consumption and training time with uniform frame sampling baselines (12 frames for low frame rate, 48 frames for high frame rate). KeyVID requires 36.4 GB VRAM and 2 min 34 s per epoch, similar to the 12-frame baseline (28.9 GB, 2 min 25 s) while achieving superior motion capture. Directly training a 48-frame model demands 52.5 GB VRAM and 8 min 48 s, although performance is still closer to KeyVID. This highlights KeyVID as a more memory-efficient model to high-frame-rate training while maintaining strong performance.

Input	Model	FID↓	IA↑	IT↑	FVD↓	AlignSync↑	RelSync↑
I+T	I2VD [66]	9.1	-	13.42	425.0	22.05	44.58
	DynamiCrafter [55]	12.4	-	1373	337.71	22.82	45.85
I+T+A	AVSyncD [66]	<b>8.7</b>	12.07	13.31	249.3	22.83	45.95
	<b>KeyVID (Ours)</b>	12.1	<b>12.40</b>	<b>15.66</b>	<b>202.1</b>	<b>22.91</b>	<b>46.03</b>
	Static	-	13.33	16.56	348.9	24.36	48.73
	Groundtruth	-	13.52	16.49	-	25.02	50.00

Table 2. Performance on *The Greatest Hit*.

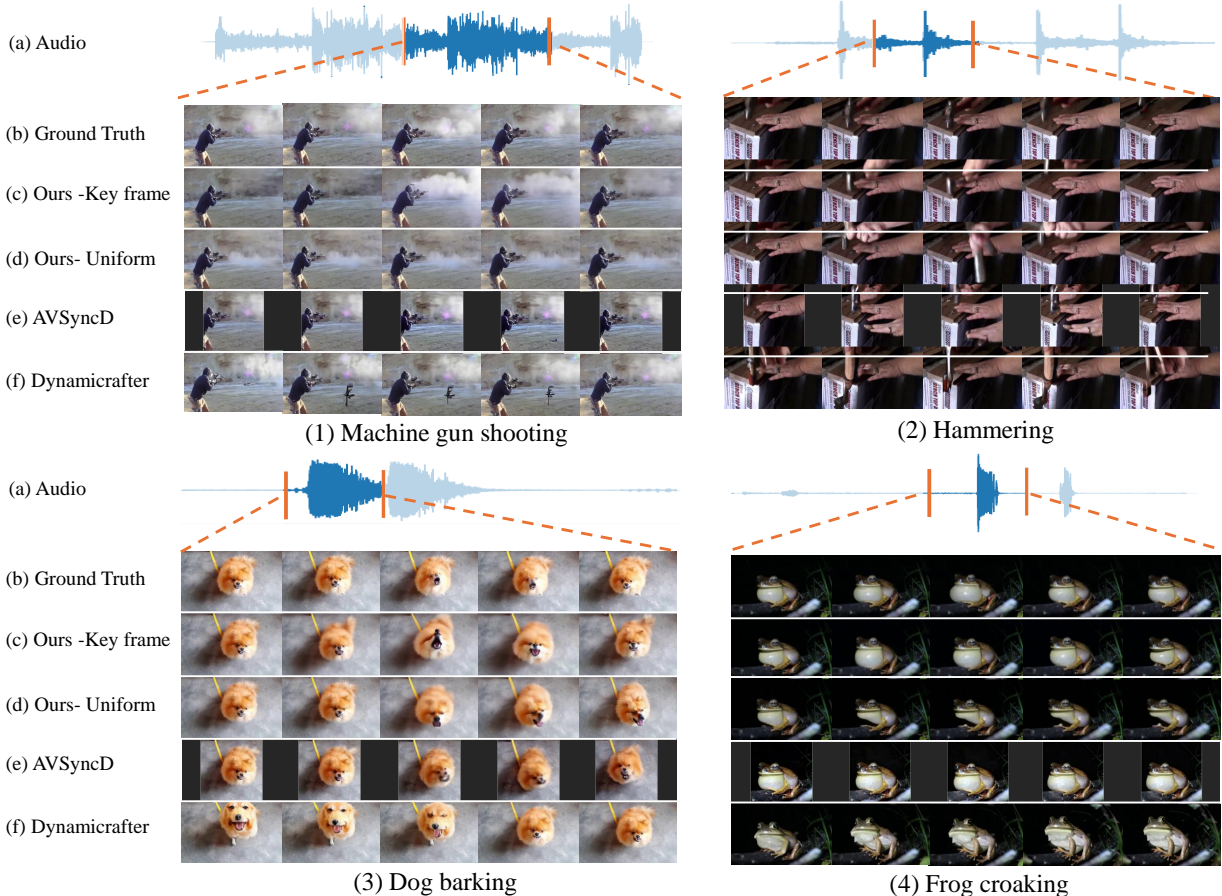


Figure 5. Qualitative comparison of KeyVID and baseline methods. We crop a key motions on audio waveform in (a) and the corresponding ground truth video in (b) as references and compare the generated video clip between models from (c) to (f). Compared with other models, our KeyVID with keyframe awareness in (c) have better alignment of the motion peaks with audio signals, for example, hitting the hammering, smoke in gun shooting, or facial changes when dogs and frogs when they make sound.

#### 4.6. Effects of Motion Intensity

To further analyze how KeyVID enhances audio synchronization across different types of motion, we compare the RelSync score across categories with varying motion intensities. As defined in Sec. 3.1, the motion score quantifies the movement within a video clip. We compute the average motion score across all instances within each category to represent its motion intensity. By ranking the 15 categories based on their motion intensity, we classify them into three levels: *Subtle*, *Moderate*, and *Intense*, with each level containing five categories. The *Intense* level includes high-dynamic motions such as hammering and dog barking, while

the *Subtle* category consists of activities with minimal movement, such as playing the violin or trumpet.

In Fig. 6, we present the RelSync metric across three motion intensity levels, comparing KeyVID, KeyVID-Uniform, and the AVSyncD baseline. Compared to KeyVID-Uniform, introducing keyframes yields a larger improvement as motion intensity increases. Specifically, KeyVID improves RelSync by 0.22 for *Subtle* motion, 1.11 for *Moderate*, and 1.66 for *Intense*, demonstrating its effectiveness in capturing rapid motion transitions. Compared to AVSyncD, our keyframe-based approach consistently outperforms it across all motion intensities. KeyVID achieves an ab-

Setting	FID↓	FVD↓	AlignSync↑	RelSync↑
<i>Evaluate on 12 frame</i>				
<b>KeyVID</b>	<b>11.00</b>	<b>262.34</b>	<b>24.08</b>	<b>48.33</b>
Uni. 12	11.01	273.40	23.53	47.23
Uni. 48	11.08	259.64	24.66	49.51
<i>Evaluate on 48 frame</i>				
<b>KeyVID</b>	<b>4.83</b>	<b>335.68</b>	<b>24.08</b>	<b>48.37</b>
Uni. 12	4.90	337.10	23.96	48.09
Uni. 48	4.81	319.26	24.91	49.94

Table 3. To demonstrate the effect of keyframe, the ablation study train the model with 12 uniform (Uni.) frames and 48 uniform frames. Each setting generate 48 frames with 24 fps, where KeyVID and Uni. 12 use the same interpolation network to increase frame length.

solute RelSync gain of 2.58 for *Subtle*, 2.70 for *Moderate*, and 2.72 for *Intense*, highlighting its superior synchronization capability compared with the baseline model.

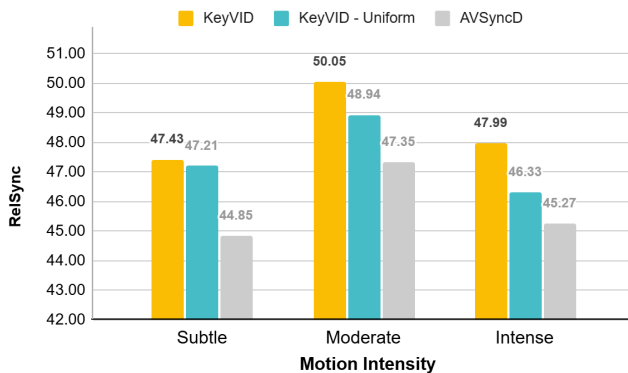


Figure 6. RelSync scores across different motion intensity levels, comparing KeyVID, KeyVID-Uniform, and AVSyncD. Our keyframe-based approach achieves the highest synchronization performance, with greater improvements over KeyVID-Uniform as motion intensity increases.

## 4.7. User Study

We conducted a user study with 12 participants to assess the perceived quality and synchronization of videos generated by different methods. Each participant was shown 20 randomly selected video samples, where each sample contained results from four models presented in a randomly ordered row with the same audio. They were asked to choose which video exhibited better audio-visual synchronization, visual quality, and temporal consistency. We aggregated all  $12 \times 20 = 240$  votes for each metric and computed the proportion of votes each model received, as shown in Tab. 4. Further details on the user study can be found in the Appendix F.

## 4.8. Open-Domain Visual Animation

We demonstrate that our model, KeyVID, has the capability to animate open-domain scenarios. The keyframe-aware model ef-

Models	AS	VQ	TC
<b>KeyVID</b>	<b>66.25%</b>	<b>65.00%</b>	<b>65.00%</b>
KeyVID-Uniform	17.92%	22.08%	21.67%
AVSyncD	11.67%	7.08%	7.92%
DynamiCrafter	4.17%	5.83%	5.42%

Table 4. User study results. Participants voted for the best method based on audio synchronization (AS), visual quality (VQ), and temporal consistency (TC). The values represent the proportion of votes each model received for each metric.

fectively captures motion dynamics and semantic meaning from audio input. As shown in Fig. 7, we select the first frame from a video clip generated by Sora and control the motion using two hammering audio clips from AVSync15. The first audio clip represents hammer strikes on a wooden surface, while the second corresponds to four hammer strikes on a metal object. The results demonstrate that our model not only generates videos with the correct pattern of hammer strikes but also adapts the motion based on the material properties inferred from the audio. These examples are best understood through visual and auditory inspection; please refer to the supplementary material to watch the videos.

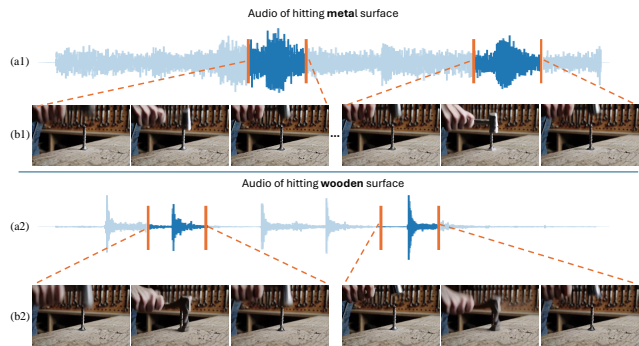


Figure 7. Open-domain motion generation results. Given the same first frame and different audio input (a1) and (a2), our model synthesizes motion that aligns with the audio’s semantics and strike pattern in (b1) and (b2). The top row shows hammering on metal nails, while the bottom row shows hammering on a wooden table.

## 5. Conclusion

In this paper, we introduced a keyframe-aware audio-synchronized visual animation model which enhances video generation quality and audio alignment, particularly for highly dynamic motions. Our approach first localizes keyframes from audio and generates corresponding frames using a diffusion model. Then we synthesizes intermediate frames to obtain smooth high-frame-rate videos while maintaining memory efficiency. Experimental results demonstrate superior performance across multiple datasets, especially in scenarios with instensive motion. Compared to previous methods, our model significantly improves audio-visual synchronization and visual quality.

## References

- [1] Kirolos Ataallah, Xiaoqian Shen, Eslam Abdelrahman, Essam Sleiman, Mingchen Zhuge, Jian Ding, Deyao Zhu, Jürgen Schmidhuber, and Mohamed Elhoseiny. Goldfish: Vision-language understanding of arbitrarily long videos. In *European Conference on Computer Vision*, pages 251–267. Springer, 2024. 3
- [2] Mohammad Babaeizadeh, Chelsea Finn, Dumitru Erhan, Roy Campbell, and Sergey Levine. Stochastic variational video prediction. In *International Conference on Learning Representations (ICLR)*, 2018. 2
- [3] Andreas Blattmann, Tim Dockhorn, Sumith Kulal, Daniel Mendelevitch, Maciej Kilian, Dominik Lorenz, Yam Levi, Zion English, Vikram Voleti, Adam Letts, et al. Stable video diffusion: Scaling latent video diffusion models to large datasets. *arXiv preprint arXiv:2311.15127*, 2023. 1, 2, 4, 5
- [4] Andreas Blattmann, Robin Rombach, Huan Ling, Tim Dockhorn, Seung Wook Kim, Sanja Fidler, and Karsten Kreis. Align your latents: High-resolution video synthesis with latent diffusion models. In *Proceedings of the IEEE/CVF conference on computer vision and pattern recognition*, pages 22563–22575, 2023. 1, 2, 4
- [5] Honglie Chen, Weidi Xie, Andrea Vedaldi, and Andrew Zisserman. Vggsound: A large-scale audio-visual dataset. In *ICASSP 2020-2020 IEEE International Conference on Acoustics, Speech and Signal Processing (ICASSP)*, pages 721–725. IEEE, 2020. 5
- [6] Haoxin Chen, Menghan Xia, Yingqing He, Yong Zhang, Xiaodong Cun, Shaoshu Yang, Jinbo Xing, Yaofang Liu, Qifeng Chen, Xintao Wang, et al. Videocrafter1: Open diffusion models for high-quality video generation. *arXiv preprint arXiv:2310.19512*, 2023. 1, 2, 5
- [7] Haoxin Chen, Yong Zhang, Xiaodong Cun, Menghan Xia, Xintao Wang, Chao Weng, and Ying Shan. Videocrafter2: Overcoming data limitations for high-quality video diffusion models, 2024. 1, 2
- [8] Rui Chen, Yixiao Li, Yifan Zhang, Hao Wang, and Yun Fu. Customizing text-to-video generation with multiple subjects. *arXiv preprint arXiv:2307.23456*, 2023. 2
- [9] Ruixiang Chen, Zhenghao Liu, and Junyan Zhou. Unitalker: A unified framework for audio-driven talking head generation. *arXiv preprint arXiv:2408.00762*, 2024. 3
- [10] Sanyuan Chen, Yu Wu, Chengyi Wang, Shujie Liu, Daniel Tompkins, Zhuo Chen, Wanxiang Che, Xiangzhan Yu, and Furu Wei. BEATs: Audio pre-training with acoustic tokenizers. In *Proceedings of the 40th International Conference on Machine Learning*, pages 5178–5193. PMLR, 2023. 3
- [11] Benjamin Elizalde, Soham Deshmukh, Mahmoud Al Ismail, and Huaming Wang. Clap learning audio concepts from natural language supervision. In *ICASSP 2023-2023 IEEE International Conference on Acoustics, Speech and Signal Processing (ICASSP)*, pages 1–5. IEEE, 2023. 3
- [12] Weichen Fan, Chenyang Si, Junhao Song, Zhenyu Yang, Yinan He, Long Zhuo, Ziqi Huang, Ziyue Dong, Jingwen He, Dongwei Pan, et al. Vchitect-2.0: Parallel transformer for scaling up video diffusion models. *arXiv preprint arXiv:2501.08453*, 2025. 1, 2
- [13] Jean-Yves Franceschi, Edouard Delasalles, Mickaël Chen, Sylvain Lamprier, and Patrick Gallinari. Stochastic latent residual video prediction. In *International Conference on Machine Learning (ICML)*, pages 3233–3246, 2020. 2
- [14] Zichen Geng, Caren Han, Zeeshan Hayder, Jian Liu, Mubarak Shah, and Ajmal Mian. Text-guided 3d human motion generation with keyframe-based parallel skip transformer. *arXiv preprint arXiv:2405.15439*, 2024. 3
- [15] Rohit Girdhar, Alaaeldin El-Nouby, Zhuang Liu, Mannat Singh, Kalyan Vasudev Alwala, Armand Joulin, and Ishan Misra. Imagebind: One embedding space to bind them all. In *Proceedings of the IEEE/CVF Conference on Computer Vision and Pattern Recognition*, pages 15180–15190, 2023. 3, 5, 6
- [16] Yuwei Guo, Ceyuan Yang, Anyi Rao, Zhengyang Liang, Yaohui Wang, Yu Qiao, Maneesh Agrawala, Dahua Lin, and Bo Dai. Animatediff: Animate your personalized text-to-image diffusion models without specific tuning. In *ICLR*, 2024. 1, 2
- [17] Yingqing He, Tianyu Yang, Yong Zhang, Ying Shan, and Qifeng Chen. Latent video diffusion models for high-fidelity long video generation. 2022. 1, 2
- [18] Amir Hertz, Ron Mokady, Jay Tenenbaum, Kfir Aberman, Yael Pritch, and Daniel Cohen-Or. Prompt-to-prompt image editing with cross-attention control. In *International Conference on Learning Representations (ICLR)*, 2023. 3
- [19] Martin Heusel, Hubert Ramsauer, Thomas Unterthiner, Bernhard Nessler, and Sepp Hochreiter. Gans trained by a two time-scale update rule converge to a local nash equilibrium. *Advances in neural information processing systems*, 30, 2017. 6
- [20] Jonathan Ho, William Chan, Chitwan Saharia, Jay Whang, Ruiqi Gao, Alexey A. Gritsenko, Diederik P. Kingma, Ben Poole, Mohammad Norouzi, David J. Fleet, and Tim Salimans. Imagen video: High definition video generation with diffusion models. *ArXiv*, abs/2210.02303, 2022. 2
- [21] Jonathan Ho, Tim Salimans, Alexey Gritsenko, William Chan, Mohammad Norouzi, and David J Fleet. Video diffusion models. *Advances in Neural Information Processing Systems*, 35:8633–8646, 2022. 1, 2
- [22] Wenyi Hong, Ming Ding, Wendi Zheng, Xinghan Liu, and Jie Tang. Cogvideo: Large-scale pretraining for text-to-video generation via transformers. *arXiv preprint arXiv:2205.15868*, 2022. 1, 2
- [23] Yujin Jeong, Wonjeong Ryoo, Seunghyun Lee, Dabin Seo, Wonmin Byeon, Sangpil Kim, and Jinkyu Kim. The power of sound (tpos): Audio reactive video generation with stable diffusion. In *Proceedings of the IEEE/CVF International Conference on Computer Vision*, pages 7822–7832, 2023. 3, 5, 6
- [24] Youngjae Jeong, Won Jeong Ryoo, Seung Hyun Lee, Donghyeon Seo, Wonmin Byeon, Sangpil Kim, and Jinkyu Kim. The power of sound (TPoS): Audio reactive video generation with stable diffusion. In *Proceedings of the IEEE/CVF International Conference on Computer Vision*, pages 7822–7832, 2023. 3, 6

- [25] Sung-Bin Kim, Arda Senocak, Hyunwoo Ha, Andrew Owens, and Tae-Hyun Oh. Sound to visual scene generation by audio-to-visual latent alignment. In *IEEE/CVF Conference on Computer Vision and Pattern Recognition (CVPR)*, 2023. 3
- [26] Sourabh Kulhare, Shagan Sah, Suhas Pillai, and Raymond Ptucha. Key frame extraction for salient activity recognition. In *2016 23rd International Conference on Pattern Recognition (ICPR)*, pages 835–840. IEEE, 2016. 3
- [27] Seungwoo Lee, Chaerin Kong, Donghyeon Jeon, and Nojun Kwak. Aadiff: Audio-aligned video synthesis with text-to-image diffusion. *arXiv preprint arXiv:2305.04001*, 2023. 3, 6
- [28] Sanghyeok Lee, Joonmyung Choi, and Hyunwoo J Kim. Multi-criteria token fusion with one-step-ahead attention for efficient vision transformers. In *Proceedings of the IEEE/CVF Conference on Computer Vision and Pattern Recognition*, pages 15741–15750, 2024. 3
- [29] Seung Hyun Lee, Gyeongrok Oh, Wonmin Byeon, Chanyoung Kim, Won Jeong Ryoo, Sang Ho Yoon, Hyunjun Cho, Jihyun Bae, Jinkyu Kim, and Sangpil Kim. Sound-guided semantic video generation. In *European Conference on Computer Vision*, pages 34–50. Springer, 2022. 3, 5
- [30] Yixiao Li, Hao Wang, Yifan Zhang, and Yun Fu. ID-Animator: Zero-shot identity-preserving human video generation. *arXiv preprint arXiv:2306.67890*, 2023. 2
- [31] Zhen Li, Lei Zhao, and Junsong Wang. Content and style aware audio-driven facial animation. *arXiv preprint arXiv:2408.07005*, 2024. 3
- [32] Zhengxiong Luo, Dayou Chen, Yingya Zhang, Yan Huang, Liang Wang, Yujun Shen, Deli Zhao, Jingren Zhou, and Tieniu Tan. Videofusion: Decomposed diffusion models for high-quality video generation. *arXiv preprint arXiv:2303.08320*, 2023. 2
- [33] Evonne Ng, Javier Romero, Timur Bagautdinov, Shaojie Bai, Trevor Darrell, Angjoo Kanazawa, and Alexander Richard. From audio to photoreal embodiment: Synthesizing humans in conversations. In *ArXiv*, 2024. 3
- [34] Andrew Owens, Phillip Isola, Josh McDermott, Antonio Torralba, Edward H Adelson, and William T Freeman. Visually indicated sounds. In *Proceedings of the IEEE conference on computer vision and pattern recognition*, pages 2405–2413, 2016. 5
- [35] Haonan Qiu, Menghan Xia, Yong Zhang, Yingqing He, Xintao Wang, Ying Shan, and Ziwei Liu. Freenoise: Tuning-free longer video diffusion via noise rescheduling. *arXiv preprint arXiv:2310.15169*, 2023. 5, 2
- [36] Alec Radford, Jong Wook Kim, Chris Hallacy, Aditya Ramesh, Gabriel Goh, Sandhini Agarwal, Girish Sastry, Amanda Askell, Pamela Mishkin, Jack Clark, et al. Learning transferable visual models from natural language supervision. In *International conference on machine learning*, pages 8748–8763. PmLR, 2021. 2, 5, 6
- [37] Colin Raffel, Noam Shazeer, Adam Roberts, Katherine Lee, Sharan Narang, Michael Matena, Yanqi Zhou, Wei Li, and Peter J Liu. Exploring the limits of transfer learning with a unified text-to-text transformer. *Journal of machine learning research*, 21(140):1–67, 2020. 2
- [38] Alexander Richard, Evgenia Egorova, Stanimir Matuszewski, Florian Bernard, Jürgen Gall, and Gerard Pons-Moll. Audio-driven 3d facial animation from in-the-wild videos. *arXiv preprint arXiv:2306.11541*, 2023. 3
- [39] Ludan Ruan, Yunzhi Ma, Hongjie Yang, Haoxian He, Bing Liu, Jianlong Fu, Nenghai Yuan, Qin Jin, and Bing Guo. MM-Diffusion: Learning multi-modal diffusion models for joint audio and video generation. In *Proceedings of the IEEE/CVF Conference on Computer Vision and Pattern Recognition*, pages 14012–14021, 2023. 3
- [40] Xiaoqian Shen, Yunyang Xiong, Changsheng Zhao, Lemeng Wu, Jun Chen, Chenchen Zhu, Zechun Liu, Fanyi Xiao, Balakrishnan Varadarajan, Florian Bordes, et al. Longvu: Spatiotemporal adaptive compression for long video-language understanding. *arXiv preprint arXiv:2410.17434*, 2024. 3
- [41] Uriel Singer, Adam Polyak, Thomas Hayes, Xi Yin, Jie An, Songyang Zhang, Qiyuan Hu, Harry Yang, Oron Ashual, Oran Gafni, Devi Parikh, Sonal Gupta, and Yaniv Taigman. Make-a-video: Text-to-video generation without text-video data. In *The Eleventh International Conference on Learning Representations*, 2023. 1, 2
- [42] Xusen Sun, Longhao Zhang, Hao Zhu, Peng Zhang, Bang Zhang, Xinya Ji, Kangneng Zhou, Daiheng Gao, Liefeng Bo, and Xun Cao. Vividtalk: One-shot audio-driven talking head generation based on 3d hybrid prior. *arXiv preprint arXiv:2312.01841*, 2023. 3
- [43] Xusen Sun, Hao Zhu, Longhao Zhang, Daiheng Gao, and Xun Cao. Echomimic: Enhancing audio-driven portrait video generation via landmark-guided fusion. *arXiv preprint arXiv:2407.08136*, 2024. 3
- [44] Kim Sung-Bin, Lee Chae-Yeon, Gihun Son, Oh Hyun-Bin, Janghoon Ju, Suekyeong Nam, and Tae-Hyun Oh. Multitalk: Enhancing 3d talking head generation across languages with multilingual video dataset. *arXiv preprint arXiv:2406.14272*, 2024. 3
- [45] Zineng Tang, Ziyi Yang, Mahmoud Khademi, Yang Liu, Chenguang Zhu, and Mohit Bansal. CoDi-2: In-context, interleaved, and interactive any-to-any generation. *arXiv preprint arXiv:2311.18775*, 2023. 3
- [46] Zhaohan Tang, Zhilin Yang, Chenguang Zhu, Michael Zeng, and Mohit Bansal. Any-to-any generation via composable diffusion. In *Thirty-seventh Conference on Neural Information Processing Systems (NeurIPS)*, 2023. 6
- [47] Zhaohan Tang, Ziyi Yang, Chenguang Zhu, Michael Zeng, and Mohit Bansal. CoDi: Any-to-any generation via composable diffusion. *arXiv preprint arXiv:2305.11846*, 2023. 3, 6
- [48] Zachary Teed and Jia Deng. Raft: Recurrent all-pairs field transforms for optical flow. In *Computer Vision—ECCV 2020: 16th European Conference, Glasgow, UK, August 23–28, 2020, Proceedings, Part II 16*, pages 402–419. Springer, 2020. 3
- [49] Thomas Unterthiner, Sjoerd Van Steenkiste, Karol Kurach, Raphael Marinier, Marcin Michalski, and Sylvain Gelly. Towards accurate generative models of video: A new metric & challenges. *arXiv preprint arXiv:1812.01717*, 2018. 2, 6
- [50] Vikram Voleti, Alexia Jolicoeur-Martineau, and Chris Pal. MCVD: Masked conditional video diffusion for prediction,

- generation, and interpolation. In *Advances in Neural Information Processing Systems (NeurIPS)*, 2022. 2
- [51] Yujie Wei, Shiwei Zhang, Zhiwu Qing, Hangjie Yuan, Zhiheng Liu, Yu Liu, Yingya Zhang, Jingren Zhou, and Hongming Shan. Dreamvideo: Composing your dream videos with customized subject and motion. *arXiv preprint arXiv:2312.04433*, 2023. 2
- [52] Shengqiong Wu, Hao Fei, Leigang Qu, Wei Ji, and Tat-Seng Chua. NExT-GPT: Any-to-any multimodal large language model. *arXiv preprint arXiv:2310.14547*, 2023. 3
- [53] Tao Wu, Yong Zhang, Xintao Wang, Xianpan Zhou, Guangcong Zheng, Zhongang Qi, Ying Shan, and Xi Li. Customcrafter: Customized video generation with preserving motion and concept composition abilities. *arXiv preprint arXiv:2408.13239*, 2024. 2
- [54] Yifan Wu, Zhen Li, and Lei Zhao. Takin-ada: Towards high-quality audio-driven talking head generation. *arXiv preprint arXiv:2410.14283*, 2024. 3
- [55] Jinbo Xing, Menghan Xia, Yong Zhang, Haoxin Chen, Wangbo Yu, Hanyuan Liu, Gongye Liu, Xintao Wang, Ying Shan, and Tien-Tsin Wong. Dynamicrafter: Animating open-domain images with video diffusion priors. In *European Conference on Computer Vision*, pages 399–417. Springer, 2024. 1, 2, 3, 4, 5, 6, 7
- [56] Mingze Xu, Mingfei Gao, Zhe Gan, Hong-You Chen, Zhengfeng Lai, Haiming Gang, Kai Kang, and Afshin Dehghan. Slowfast-llava: A strong training-free baseline for video large language models. *arXiv preprint arXiv:2407.15841*, 2024. 3
- [57] Ling Yang, Zhilong Zhang, Yang Song, Shenda Hong, and Runsheng Xu. Diffusion-based video generation with image prompts. *arXiv preprint arXiv:2305.12345*, 2023. 2
- [58] Shiqing Yang, Bo Li, and Xiaoming Wang. Emoface: Emotionally expressive audio-driven talking heads. *arXiv preprint arXiv:2407.12501*, 2024. 3
- [59] Xiaodong Yang, Yixiao Li, Yifan Zhang, and Yun Fu. Cogvideox: Extending video generation with advanced controls. *arXiv preprint arXiv:2403.34567*, 2024. 1, 2
- [60] Guy Yariv, Itai Gat, Sagie Benaim, Lior Wolf, Idan Schwartz, and Yossi Adi. Diverse and aligned audio-to-video generation via text-to-video model adaptation. *arXiv preprint arXiv:2303.13841*, 2023. 3
- [61] Guy Yariv, Itai Gat, Sagie Benaim, Lior Wolf, Idan Schwartz, and Yossi Adi. Diverse and aligned audio-to-video generation via text-to-video model adaptation. In *Proceedings of the AAAI Conference on Artificial Intelligence*, pages 6639–6647, 2024. 5, 6
- [62] Shengming Yin, Chenfei Wu, Huan Yang, Jianfeng Wang, Xiaodong Wang, Minheng Ni, Zhengyuan Yang, Linjie Li, Shuguang Liu, Fan Yang, Jianlong Fu, Gong Ming, Lijuan Wang, Zicheng Liu, Houqiang Li, and Nan Duan. NUWA-XL: Diffusion over diffusion for extremely long video generation. *arXiv preprint arXiv:2303.12346*, 2023. 3
- [63] David Junhao Zhang, Jay Zhangjie Wu, Jia-Wei Liu, Rui Zhao, Lingmin Ran, Yuchao Gu, Difei Gao, and Mike Zheng Shou. Show-1: Marrying pixel and latent diffusion models for text-to-video generation. *arXiv preprint arXiv:2309.15818*, 2023. 2
- [64] Hao Zhang, Qian Jiang, Xiang Li, and Hao Wang. Lingualinker: Multilingual audio-driven talking head synthesis. *arXiv preprint arXiv:2407.18595*, 2024. 3
- [65] Jiangning Zhang, Chao Xu, Liang Liu, Mengmeng Wang, Xia Wu, Yong Liu, and Yunliang Jiang. DTVNet: Dynamic time-lapse video generation via single still image. In *Proceedings of the European Conference on Computer Vision (ECCV)*, pages 300–315, 2020. 2
- [66] Lin Zhang, Shentong Mo, Yijing Zhang, and Pedro Morgado. Audio-synchronized visual animation. In *European Conference on Computer Vision*, pages 1–18. Springer, 2024. 1, 2, 3, 5, 6, 7
- [67] Mingzhe Zheng, Yongqi Xu, Haojian Huang, Xuran Ma, Yexin Liu, Wenjie Shu, Yatian Pang, Feilong Tang, Qifeng Chen, Harry Yang, and Ser-Nam Lim. Videogen-of-thought: A collaborative framework for multi-shot video generation. *arXiv preprint arXiv:2412.02259*, 2024. 3
- [68] Daquan Zhou, Weimin Wang, Hanshu Yan, Weiwei Lv, Yizhe Zhu, and Jiashi Feng. Magicvideo: Efficient video generation with latent diffusion models. *arXiv preprint arXiv:2211.11018*, 2022. 2

# KeyVID: Keyframe-Aware Video Diffusion for Audio-Synchronized Visual Animation

## Supplementary Material

### A. Details of Keyframe Localization Network from Audio

In the Sec. 3.1 of main paper, we introduce that we need to know the position of key frame at the begin of inference by predicting optical motion scores. Here is the detailed structure of this network. The network processes raw audio by converting it into a spectrogram  $\mathbf{A} \in \mathbb{R}^{C_A \times T_A}$ , where  $C_A$  denotes the number of frequency channels and  $T_A$  represents the temporal length. The original ImageBind preprocessing pipeline applies a CNN with a kernel stride of (10, 10) to patchify the input spectrogram, producing feature embeddings that are then processed by a transformer-based encoder  $f_{\text{audio}} \in \mathbb{R}^{B \times T \times C}$ . However, this results in  $T$  (e.g.  $T=19$ ) being misaligned with the temporal resolution of the dense motion curve sequence (e.g. 48).

To address this, we modify the CNN stride to (10, 4), increasing the temporal resolution of extracted features (e.g. increase to 46). The transformer encoder then processes the updated feature sequence:

$$\mathbf{F}_{\text{audio}} = f_{\text{audio}}(\mathbf{A}), \quad \mathbf{F}_{\text{audio}} \in \mathbb{R}^{B \times T' \times C}, \quad (5)$$

where  $T' > T$  reflects the increased temporal resolution. Since the transformer relies on positional embeddings, we interpolate the pretrained positional embeddings to match the new sequence length  $T'_A$  and keep them frozen during training.

The extracted features are passed through fully connected layers to predict a sequence of confidence scores  $\mathbf{s} \in \mathbb{R}^{B \times T'}$ , where each  $s_t$  represents the likelihood of a keyframe occurring at time step  $t$ :

$$\mathbf{s} = \sigma(\mathbf{W}\mathbf{F}_{\text{audio}} + \mathbf{b}), \quad (6)$$

where  $\mathbf{W} \in \mathbb{R}^{C \times 1}$  and  $\mathbf{b} \in \mathbb{R}^{T'_A}$  are learnable parameters, and  $\sigma(\cdot)$  is the sigmoid activation function. The model is trained using an L1 loss:

$$\mathcal{L} = \|\mathbf{s} - \hat{\mathbf{s}}\|_1, \quad (7)$$

where  $\hat{\mathbf{s}}$  represents the ground-truth keyframe labels derived from optical flow analysis.

### B. Details of Keyframe Selection

#### B.1. Detect Peak and Valley

To identify the local maxima (*peaks*) and minima (*valleys*) from a one-dimensional motion score  $\{M(t)\}_{t=1}^T$ , we perform the following steps:

1. **Smoothing:** Convolve the raw score  $M(t)$  with a short averaging filter with a window size 5, producing a smoothed label  $\bar{M}(t)$ . This helps reduce noise and minor fluctuations.
2. **Peak Detection:** Finds all local maxima by simple comparison of neighboring values for  $\bar{M}(t)$ . We force a minimum distance

of 5 frames between any two detected peaks and requiring a prominence (height relative to its surroundings) of at least 0.1. This returns the indices of the local maxima.

3. **Valley Detection:** Repeat the same peak-finding procedure on the negative of the smoothed signal.

#### B.2. Sample keyframes

In the main text, we discuss the process of selecting  $T_K \ll T$  keyframes based on the motion score  $M(t)$  for each frame. Specifically, we first pick the initial frame, then select up to  $\frac{T_K}{2} - 1$  peaks among all detected ones (or all peaks if fewer are found). Next, we include a valley between each consecutive pair of selected peaks. Finally, we sample any remaining frames by an evenly distributed (proportional) strategy, which approximates uniform downsampling if few peaks and valleys are present. This approach ensures that smooth motion or weak audio signals, producing limited peaks and valleys, do not degrade the consistency of training for video diffusion models.

Algorithm 1 is the detailed pseudo-code for the full procedure, including both peak and valley selection and the final proportional allocation of remaining key frames.

### C. Structure of Motion Interpolation

As shown in Fig. 8, we present the pipeline of motion interpolation network as introduced in Sec. 3.3

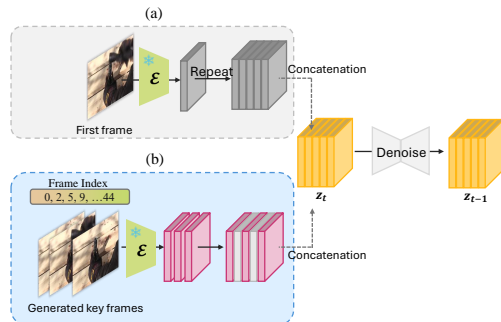


Figure 8. The frame interpolation models has the same structure as the original keyframe generation model, but has different image features for concatenation. (a) For the keyframe generation in Sec 3.2, the first frame features are repeated to match the frame length of the latent vector; (b) In frame interpolation, the condition feature from keyframes are padded with zero tensor between keyframe locations to match the frame length.

### D. Motion score prediction evaluation

**Quantitative result.** We evaluate the keypoint detected from the predicted motion score with the ground truth score. We calculate

---

**Algorithm 1: Keyframe Selection Algorithm**

---

**Input:** Motion scores  $\{M(t)\}_{t=1}^T$ , desired keyframe count  $T_K \ll T$ .

**Output:** A set of  $T_K$  keyframes.

- 1 **Step 1: Detect peaks and valleys** based on  $M(t)$ .
  - 2 **Step 2: Initialize keyframe list:**  
Keyframes  $\leftarrow \{\text{first\_frame}\}$ .
  - 3 **Step 3: Randomly select peaks**  
Choose up to  $\lfloor \frac{T_K}{2} - 1 \rfloor$   
from the detected peaks and add to Keyframes.
  - 4 **Step 4: Insert valleys**  
for each pair of consecutive peaks in  
Keyframes **do**  
    Select one valley in between and add it to  
    Keyframes.
  - 5 **Step 5: Compute how many more keyframes are needed:**  
     $R \leftarrow T_K - |\text{Keyframes}|$ .
  - 6 **if**  $R > 0$  **then**
    - 7 Define a list of  $N$  remaining frames (unselected) with some weights  $\{w_1, \dots, w_N\}$ .
    - 8  $W \leftarrow \sum_{i=1}^N w_i$
    - 9 **for**  $i \leftarrow 1$  **to**  $N$  **do**  
    ideal\_share $_i \leftarrow R \cdot \frac{w_i}{W}$ ;  
    allocated $_i \leftarrow \lfloor \text{ideal\_share}_i \rfloor$ ;
    - 10  $r \leftarrow R - \sum_{i=1}^N \text{allocated}_i$ ; // Remainder after flooring
    - 11 **if**  $r > 0$  **then**
      - 12 **for**  $i \leftarrow 1$  **to**  $N$  **do**  
        **for**  $i \leftarrow 1$  **to**  $N$  **do**  
            frac $_i \leftarrow \text{ideal\_share}_i - \text{allocated}_i$ ;  
            Sort frames by frac $_i$  in descending order.
      - for**  $j \leftarrow 1$  **to**  $r$  **do**  
             $i^* \leftarrow$  index of the  $j$ -th largest frac $_i$ ;  
            allocated $_{i^*} \leftarrow \text{allocated}_{i^*} + 1$ ;
  - 12 **for**  $i \leftarrow 1$  **to**  $N$  **do**  
    **if** allocated $_i > 0$  **then**  
        Keyframes  $\leftarrow \text{Keyframes} \cup \{\text{frame}_i\}$ ;
- 13 **return** Keyframes
- 

the average precision with a distance threshold  $t$ . In this way, for each keypoint in ground truth motion score curve, if it can match with a predicted keypoint with distance lower than  $t$ , it will be consider as a successful match. The average precision means the the average of  $N_{match}/N(\text{total})$  across all instance, denoted as  $AP@t$ . We achieve the  $AP@3 = 60.57\%$  and  $AP@5 = 77.92\%$ .

### Visualization

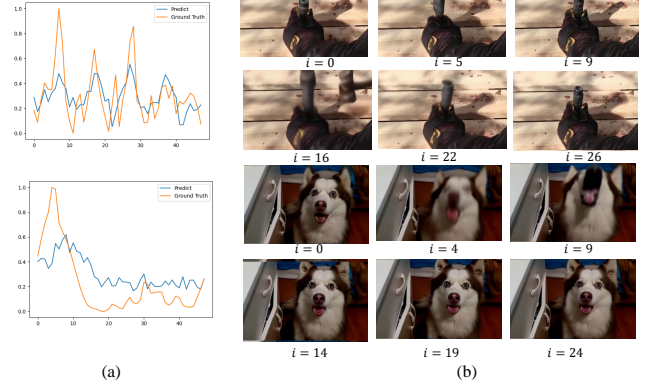


Figure 9. Visualization of (a) Predicted motion score from audio with the ground truth caluate from video data; and (b) the generated video keyframe by diffusion network described in Sec. 3.2 before interpolations.

## E. More Qualitative Results of Video Generation

As the generation result need to be watch with audio for the best experience, we have put more visualization result into the supplementary as mp4 files.

## F. Details of User Study

As described in the main paper (Sec. 4.7), we conduct a user study to evaluate the performance of four video generation models in terms of audio synchronization, visual quality, and temporal frame consistency. We invite 12 participants and design an online survey to collect responses. In the survey, we randomly select 20 video instances and present the generation results from four models—KeyVID, KeyVID-Uniform, AVSyncD, and Dynamicrafter—in a row for comparison, with the order randomly shuffled. The videos generated by KeyVID, KeyVID-Uniform, and AVSyncD use the same audio, image, and text conditions, whereas Dynamicrafter generates videos using only text and image conditions. For each instance, participants are asked to select the best video based on three evaluation metrics. This results in a total of  $20 \times 12 = 240$  votes for each metric across all models. Sample survey questions are illustrated in Fig. 10.

## G. Experimental Details

For the experiments of KeyVID on three dataset AVSyncD, Landscape, and TheGreatestHit, we all train on resolution  $320 \times 512$  as Dynamicrafter [55]. During the inference time, we use ddim sampling with step 90. The temporal length of both key frame generation and interpolation model are all 12. As our interpolation module use freenoise[35] technique to obtain the final 48 frames in one run. we change the windows size 12 and the stride 6 to fit our temporal length.

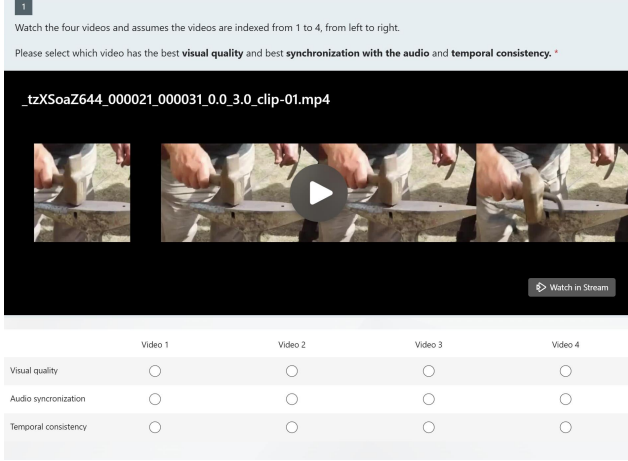


Figure 10. Sample survey question used in the user study.

## H. Multimodal Classifier Free Guidance

Similar to Xing et al. [55], we introduce three guidance scales  $s_{\text{img}}$ ,  $s_{\text{txt}}$ , and  $s_{\text{aud}}$  to extend video generation with additional audio control. These scales allow balancing the influence of different conditioning modalities in video generation. The modified noise estimation function is defined as:

$$\begin{aligned} \hat{\epsilon}_{\theta}(\mathbf{z}_t, \mathbf{c}_{\text{img}}, \mathbf{c}_{\text{txt}}, \mathbf{c}_{\text{aud}}) &= \epsilon_{\theta}(\mathbf{z}_t, \emptyset, \emptyset, \emptyset) \\ &+ s_{\text{img}} (\epsilon_{\theta}(\mathbf{z}_t, \mathbf{c}_{\text{img}}, \emptyset, \emptyset) - \epsilon_{\theta}(\mathbf{z}_t, \emptyset, \emptyset, \emptyset)) \\ &+ s_{\text{txt}} (\epsilon_{\theta}(\mathbf{z}_t, \mathbf{c}_{\text{img}}, \mathbf{c}_{\text{txt}}, \emptyset) - \epsilon_{\theta}(\mathbf{z}_t, \mathbf{c}_{\text{img}}, \emptyset, \emptyset)) \\ &+ s_{\text{aud}} (\epsilon_{\theta}(\mathbf{z}_t, \mathbf{c}_{\text{img}}, \mathbf{c}_{\text{txt}}, \mathbf{c}_{\text{aud}}) - \epsilon_{\theta}(\mathbf{z}_t, \mathbf{c}_{\text{img}}, \mathbf{c}_{\text{txt}}, \emptyset)). \end{aligned} \quad (8)$$

Here,  $\mathbf{c}_{\text{img}}$ ,  $\mathbf{c}_{\text{txt}}$ , and  $\mathbf{c}_{\text{aud}}$  represent image, text, and audio conditioning, respectively. The newly introduced audio guidance scale  $s_{\text{aud}}$  enables the model to integrate temporal audio cues, ensuring synchronized motion generation in audio-reactive video synthesis. By adjusting these guidance parameters, we can control the relative impact of each modality in the final video output.

In experiment, we choose the audio guidance scale to 7.5 and image guidance scale to 2, for both keyframe generation network and frame interpolatio network. As we add the audio guidance as a new feature, we compare the result from different audio guidance from 4.0 to 11.0 as list in Tab. 5. Although the higher audio guidance obtains a better audio synchronization score (RelSync and AlignSync) we finally choose the one with the best visual quality (FVD and FID) but still ahiveve compatible audio synchronization score.

$s_{\text{aud}}$	FID↓	FVD↓	AlignSync↑	RelSync↑
4.0	11.4	270.5	48.18	24.14
7.5	<b>11.0</b>	<b>262.3</b>	48.33	24.08
9.0	11.1	277.2	48.55	24.16
11.0	11.1	278.6	<b>48.66</b>	<b>24.22</b>

Table 5. Performance metrics for different guidance values.

## I. Details of Motion Intensity

To analyze motion intensity in AVSyncD, we cluster 15 classes based on their average motion scores across all instances. The classes are grouped into three motion intensity levels:

- **Subtle:** playing trumpet, playing violin, playing cello, machine gun, striking bowling.
- **Moderate:** lions roaring, cap gun shooting, frog croaking, chicken crowing, baby crying.
- **Intensive:** playing trombone, toilet flushing, dog barking, hammering, sharpening knife.

This classification provides insights into motion intensity distribution within AVSyncD, aiding in evaluating synchronization across different motion levels.